AMERICAN SOCIETY FOR MICROBIOLOGY | Applied and Environmental Microbiology®

ENVIRONMENTAL MICROBIOLOGY

Viral Lysis Alters the Optical Properties and Biological Availability of Dissolved Organic Matter Derived from *Prochlorococcus* Picocyanobacteria

Xilin Xiao,[a] Weidong Guo,[a] Xiaolin Li,[a] Chao Wang,[a] Xiaowei Chen,[a] Xingqin Lin,[b] Markus G. Weinbauer,[c] Qinglu Zeng,[b,d] Nianzhi Jiao,[a] Rui Zhang[a]

[a]State Key Laboratory of Marine Environmental Science, College of Ocean and Earth Sciences, Fujian Key Laboratory of Marine Carbon Sequestration, Xiamen University, Xiamen, China

[b]Division of Life Science, The Hong Kong University of Science and Technology, Clear Water Bay, Hong Kong, China

[c]Laboratoire d'Océanographie de Villefranche (LOV), Sorbonne Universités, UPMC, Université Paris 06, CNRS, Villefranche-sur-Mer, France

[d]Department of Ocean Science, The Hong Kong University of Science and Technology, Clear Water Bay, Hong Kong, China

ABSTRACT Phytoplankton contribute almost half of the world's total primary production. The exudates and viral lysates of phytoplankton are two important forms of dissolved organic matter (DOM) in aquatic environments and fuel heterotrophic prokaryotic metabolism. However, the effect of viral infection on the composition and biological availability of phytoplankton-released DOM is poorly understood. Here, we investigated the optical characteristics and microbial utilization of the exudates and viral lysates of the ecologically important unicellular picophytoplankton *Prochlorococcus*. Our results showed that *Prochlorococcus* DOM produced by viral lysis (Pro-vDOM) with phages of three different morphotypes (myovirus P-HM2, siphovirus P-HS2, and podovirus P-SSP7) had higher humic-like fluorescence intensities, lower absorption coefficients, and higher spectral slopes than DOM exuded by *Prochlorococcus* (Pro-exudate). The results indicate that viral infection altered the composition of *Prochlorococcus*-derived DOM and might contribute to the pool of oceanic humic-like DOM. Incubation with Pro-vDOM resulted in a greater dissolved organic carbon (DOC) degradation rate and lower absorption spectral slope and heterotrophic bacterial growth rate than incubation with Pro-exudate, suggesting that Pro-vDOM was more bioavailable than Pro-exudate. In addition, the stimulated microbial community succession trajectories were significantly different between the Pro-exudate and Pro-vDOM treatments, indicating that viral lysates play an important role in shaping the heterotrophic bacterial community. Our study demonstrated that viral lysis altered the chemical composition and biological availability of DOM derived from *Prochlorococcus*, which is the numerically dominant phytoplankton in the oligotrophic ocean.

IMPORTANCE The unicellular picocyanobacterium *Prochlorococcus* is the numerically dominant phytoplankton in the oligotrophic ocean, contributing to the vast majority of marine primary production. *Prochlorococcus* releases a significant fraction of fixed organic matter into the surrounding environment and supports a vital portion of heterotrophic bacterial activity. Viral lysis is an important biomass loss process of *Prochlorococcus*. However, little is known about whether and how viral lysis affects *Prochlorococcus*-released dissolved organic matter (DOM). Our paper shows that viral infection alters the optical properties (such as the absorption coefficients, spectral slopes, and fluorescence intensities) of released DOM and might contribute to a humic-like DOM pool and carbon sequestration in the ocean. Meanwhile, viral lysis also releases various intracellular labile DOM, including amino acids, protein-like DOM, and lower-molecular-weight DOM, increases the bioavailability of DOM, and

Citation Xiao X, Guo W, Li X, Wang C, Chen X, Lin X, Weinbauer MG, Zeng Q, Jiao N, Zhang R. 2021. Viral lysis alters the optical properties and biological availability of dissolved organic matter derived from *Prochlorococcus* picocyanobacteria. Appl Environ Microbiol 87:e02271-20. https://doi.org/10.1128/AEM.02271-20.

Editor Karyn N. Johnson, University of Queensland

Address correspondence to Nianzhi Jiao, Jiao@xmu.edu.cn, or Rui Zhang, ruizhang@xmu.edu.cn.

Received 16 September 2020
Accepted 3 November 2020
Accepted manuscript posted online 20 November 2020
Published 15 January 2021

shapes the successive trajectory of the heterotrophic bacterial community. Our study highlights the importance of viruses in impacting the DOM quality in the ocean.

KEYWORDS *Prochlorococcus*, bioavailability, dissolved organic matter, microbial communities, optical properties, viral lysis

As the base of the marine food web, phytoplankton account for less than 1% of the photosynthetic biomass on Earth but contribute to almost half of the world's total primary production (1, 2). Large amounts of photosynthetically fixed organic matter are released into the surrounding seawater (3–5). It has been suggested that the rates of dissolved organic matter (DOM) production by phytoplankton will increase due to warmer, more acidic, and more stratified conditions in the future ocean (6). Exudates and viral lysates are the two major sources of DOM released from phytoplankton. A significant proportion of phytoplankton are infected and lysed by viruses (5, 7, 8), thus releasing their cellular contents into the environment. Viral infections have been shown to restructure the fatty acid composition of *Emiliania huxleyi* (9). The production of DOM released by *Micromonas pusilla* was stimulated by viral infection, coupling with the change of DOM composition (4). Phytoplankton-derived DOM is highly bioavailable (10–12) and includes carbohydrates, amino acids (peptides and protein), carboxylic acids, lipids, and other cellular materials (such as pigments, polyphenols, and trace metals) (3, 13–16). This DOM is consumed primarily by heterotrophic bacterioplankton, shapes the surrounding bacterial community structure, and supports the function of the microbial loop (5, 17–20). Recently, Fang and colleagues (21) found that *Synechococcus* viral lysate may play a role as a source of organic nitrogen to regulate the transcription of the N-metabolism-related genes of uninfected cooccurring phytoplankton.

In tropical and subtropical oligotrophic oceans, the unicellular picocyanobacterium *Prochlorococcus* is the numerically dominant phytoplankton (22). Its specific divinyl-chlorophyll *a* accounts for 30 to 60% of the total chlorophyll *a* in subtropical oligotrophic oceans (23). Data from field surveys indicate that virus-mediated mortality is responsible for up to 60% of *Prochlorococcus* cell loss (8, 24, 25) and releases various DOM that serves as a large bioavailable carbon source in the vast oligotrophic oceans. It is estimated that *Prochlorococcus* releases 9 to 24% of its daily primary productivity as DOM into the surrounding environment, which supports a large part of bacterial production in oligotrophic regions (3). The chemical molecular analysis showed that the released DOM consists of low-molecular-weight (LMW) carboxylic acids, hydrocarbon, and amino acids as well as small, nonpolar materials (3, 26, 27). However, the detailed effects of virus infection on the composition and microbial utilization of DOM released from *Prochlorococcus* remain unstudied.

Prochlorococcus MED4 is an ecologically important high-light-adapted *Prochlorococcus* model strain. MED4 is distributed in the upper-middle euphotic zone and achieves numerical dominance in well-mixed, nutrient-rich, high-latitude waters (28). In this study, we conducted a microcosm experiment with DOM exuded by *Prochlorococcus* during growth (Pro-exudate) and DOM released by lysis of *Prochlorococcus* cells (Pro-vDOM) with infection of three lytic phages (myovirus P-HM2, siphovirus P-HS2, and podovirus P-SSP7). We investigated the optical properties and bioavailability of these different DOM types and the response of the microbial community to a low dose of Pro-vDOM. In recent decades, it has been demonstrated that the absorption and fluorescence properties of DOM (referring to chromophoric DOM [CDOM] and fluorescent DOM [FDOM], respectively) provide powerful indexes of DOM characteristics (29), and they have been widely used in oceanographic studies (30, 31). The chemical composition of phytoplankton-derived DOM has been studied in detail using different mass spectrometry analyses (13, 15, 27). However, it is difficult to connect such analyses with oceanographic surveys that target the optical characteristics of DOM. By combining optical characterization with the biodegradation of *Prochlorococcus*-derived DOM, our study provides fundamental data to link laboratory

TABLE 1 DOC concentration and optical properties of the DOM derived from *Prochlorococcus*

				Fluorescence intensity (RU)[a]								
				Humic-like components						Protein-like components		
DOM source	DOC (μM)	a_{254} (m^{-1})	$S_{275–295}$[b] (10^{-2} nm^{-1})	Peak A (250/466)[c]	C2 (255/456)	Peak M[b] (335/404)	C4[b] (325/396)	Peak C (355/450)	C3 (<250/368)	Peak T (270/342)	C1 (275/332)	C5 (275/300)
Pro-medium	160.9			0.19	0.12	0.09	0.08	0.06	0.13	0.15	0.13	0.04
Pro-exudate	234.0	3.37	2.88	0.36	0.36	0.22	0.22	0.20	0.19	0.25	0.24	0.08
P-HS2 lysate	259.5	3.65	3.29	0.37	0.34	0.27	0.26	0.21	0.14	0.19	0.18	0.08
P-SSP7 lysate	319.0	4.77	4.27	0.35	0.36	0.29	0.28	0.23	0.18	0.26	0.26	0.08
P-HM2 lysate	244.4	5.08	3.80	0.38	0.38	0.30	0.30	0.22	0.17	0.19	0.19	0.06

[a]The FDOM components (C1 to C5), as identified by PARAFAC modeling, are shown with the corresponding FDOM components (peaks A, M, C, and T) identified by the peak-picking method. The data shown are the means of two replicates. RU, Raman units.
[b]Significant difference between Pro-exudate and Pro-vDOM, *t* test (double tailed), $P < 0.05$.
[c]Values in parentheses are excitation/emission wavelengths.

analyses with large-scale oceanographic survey data. This work will help us understand the role of viral infection in the composition and biodegradability of phytoplankton-released DOM and improve the knowledge of the viral impact on ecology and biogeochemistry in the ocean.

RESULTS

DOM derived from *Prochlorococcus*. Dissolved organic carbon (DOC) concentrations of Pro-exudate and Pro-vDOM were much higher than that of Pro-medium (see Materials and Methods) (Table 1). The optical properties of DOM derived from *Prochlorococcus* were investigated using a UV-visible spectrophotometer and a spectrofluorometer. As shown in Table 1, the UV absorbance coefficients at 254 nm (a_{254}) of Pro-vDOM (except P-HS2 lysate) were higher than those of Pro-exudate, and the magnitude of this trend differed between the different phage types used. Our data showed that the spectral slope over the wavelength range from 275 to 295 nm ($S_{275–295}$) values of Pro-vDOM were significantly higher than those of Pro-exudate (*t* test, $P < 0.05$). This indicated that Pro-vDOM contained more LMW DOM than did Pro-exudate.

Pro-exudate and three types of Pro-vDOM shared similar fluorescence excitation-emission matrices (EEMs) (Fig. 1). According to the EEMs of Pro-DOM, *Prochlorococcus* produced both protein-like (peak T) and humic-like (peak A, C, and M) fluorescent materials through exudation and viral lysis (Table 1). Both Pro-exudate and Pro-vDOM showed the most prominent peaks at 250/466 nm (excitation/emission [ex/em]), which corresponded to previously defined "terrestrial humic-like" substances (peak A) (32). The fluorescence intensity of the peak at 335/404 nm (ex/em), which corresponds to marine humic-like materials (peak M) (32), was the second highest. Another humic-like peak assigned to peak C (ex/em, 355/450 nm) appeared in all Pro-DOM. Compared to the peaks observed for Pro-medium, peak M and peak C were the most increased components. The fluorescence intensity of peak M of Pro-vDOM was significantly higher than that of Pro-exudate (*t* test, $P < 0.05$). In the protein-like region, one peak at ex/em 270/342 nm (peak T) was found in Pro-exudate and Pro-vDOM. Podovirus P-SSP7-mediated Pro-vDOM showed the highest fluorescence intensity for protein-like peak T.

The total dissolved amino acid (TDAA) analysis showed that Asp, Glu, Ala, and Gly were the dominant amino acids in Pro-DOM (see Table S2 in the supplemental material). Compared with those of Pro-medium, the DOC-normalized TDAA of Pro-DOM were significantly elevated, and the TDAA concentrations of the P-HS2 and P-SSP7 lysates were higher than those of Pro-exudate, supporting the $S_{275–295}$ results shown above (Table 1). In addition, the total concentration of the 14 amino acids of Pro-vDOM increased differently than did that of Pro-exudate (Table S2). Together, our data showed that both the quantity and quality of DOM were different between Pro-exudate and Pro-vDOM.

Microbial utilization of DOM. After DOM addition, the initial DOC concentration of all treatments ranged from 80.4 μM (Pro-medium treatment) to 89.4 μM (P-HS2 lysate

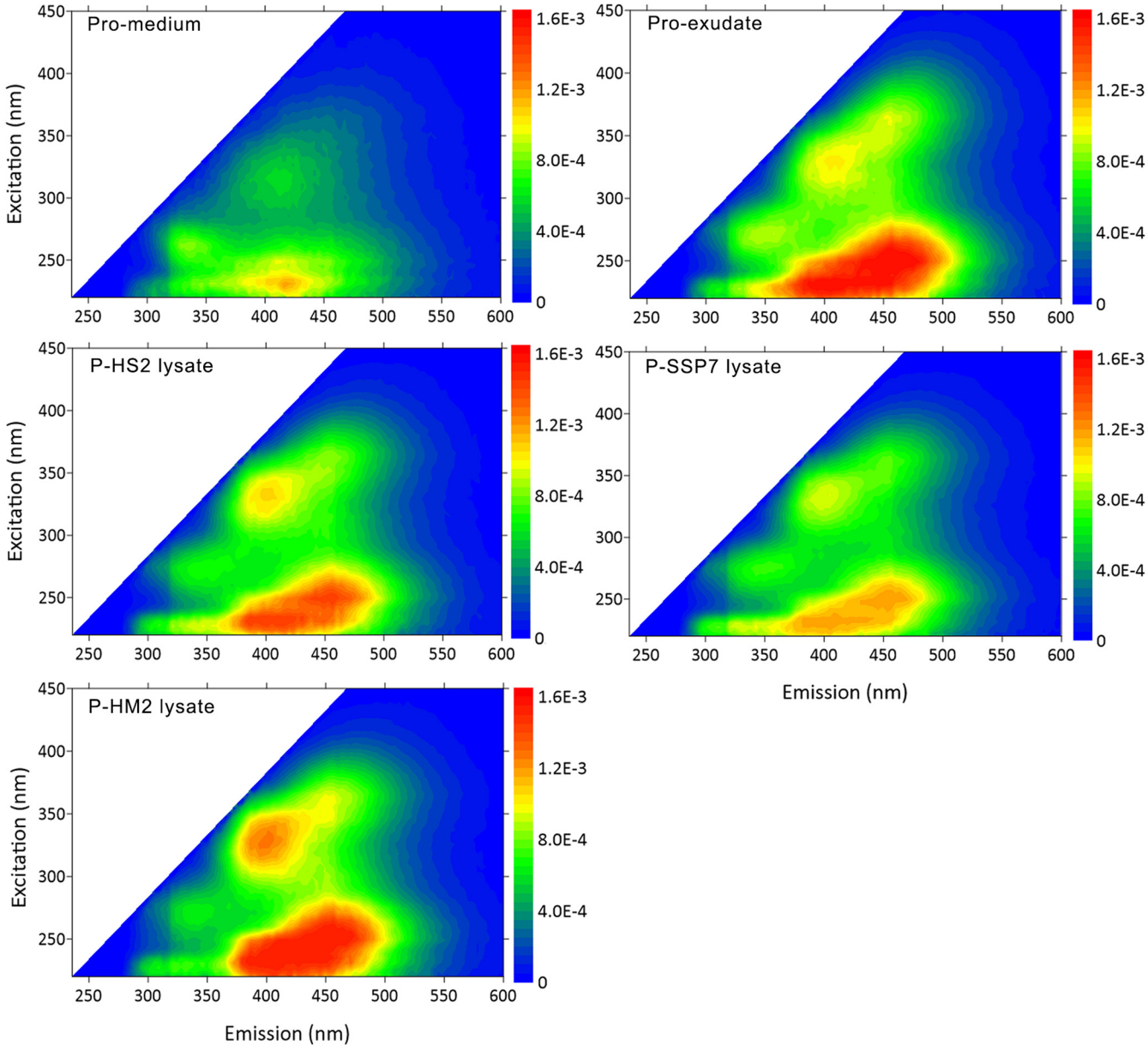

FIG 1 Viral lysis enhanced the production of fluorescent DOM derived from *Prochlorococcus*. The fluorescence intensities of the excitation-emission matrix of the five generated DOM were normalized to the DOC concentration. Units are liters μmol C^{-1} Raman units. The scale bar along each figure represents the fluorescence intensity.

treatment), corresponding to DOC increases of 7.9% to 20.0% from the DOC concentration in the control (74.4 μM) (Table S3). During the 120-h incubation experiment, the DOC concentration of the control remained stable, while those of the DOM addition treatments rapidly degraded in the first 18 h (Fig. 2a). The amount of consumed DOC ranged from 3.6 μM to 8.6 μM in the first 18 h, corresponding to 4.5% to 9.6% of the initial DOC content (Table S3). The DOC consumption ratio of Pro-vDOM was higher than that of Pro-exudate at 18 h and 120 h.

Figure 2b displays the CDOM spectral slope $S_{275-295}$ of each treatment at a specific sampling time during the incubation period. After DOM addition, the initial spectral slopes ranked as follows: control > Pro-vDOM > Pro-exudate > Pro-medium. This result suggested that the Pro-exudate treatment contained much more high-molecular-weight DOM than did the Pro-vDOM treatments at the beginning of incubation. At the end of the incubation, all DOM addition treatments had similar spectral slopes;

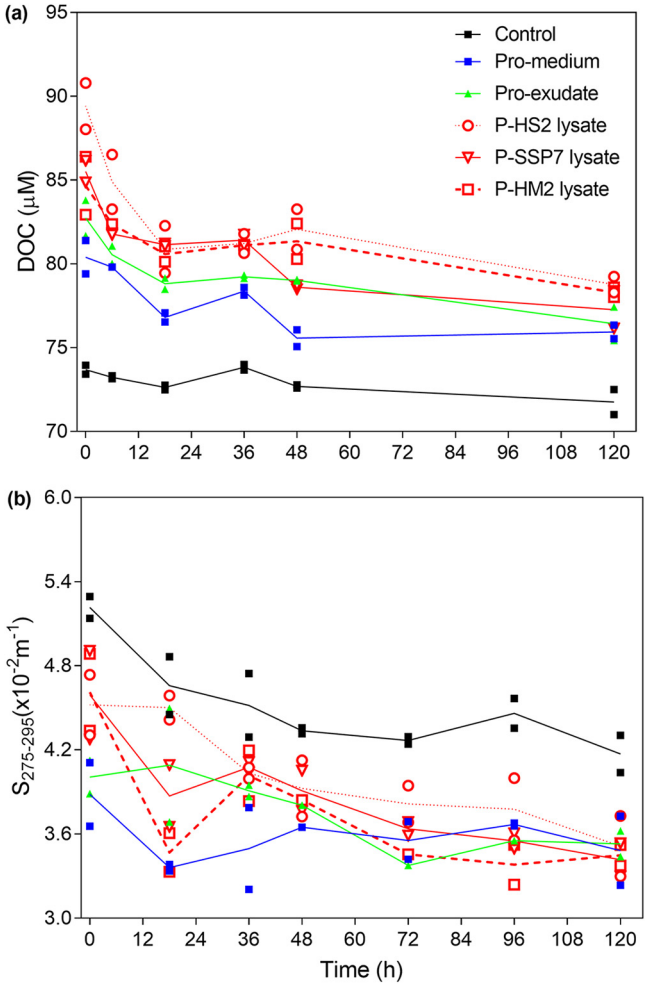

FIG 2 Changes in DOM quantity and quality after incubation with *Prochlorococcus* exudate and lysate produced by different viruses. (a) Microbial utilization of different DOC derived from *Prochlorococcus* DOM; (b) the DOM spectral slope $S_{275-295}$, which is typically related to DOM molecular weight, at specific sampling times for each DOM treatment. The value of each replicate and the trend line of each treatment are shown.

however, these slopes differed from those at the beginning (Fig. 2b), hence resulting in the spectral slope of Pro-vDOM decreasing more than that of Pro-exudate.

Five fluorescent components were identified using parallel factor analysis (PARAFAC), including two protein-like and three humic-like components (Fig. 3, left panel). Components 1 and 5 (C1 and C5) were characterized as amino acid-like DOM (32) and displayed relatively narrower emission spectra with maxima below 350 nm. C1 displayed excitation maximum at 275 nm and one emission maximum at 332 nm, which was similar to tryptophan-like peak T. C5 had an excitation/emission maximum at 275/300 nm, similar to tyrosine-like peak B. Components 2, 3, and 4 (C2, C3, and C4) were assigned to humic-like FDOM. C2 exhibited two peaks with excitation maxima at 255/365 nm and emission at 456 nm and was categorized as a combination of terrigenous humic-like peaks A and C (32). C3 exhibited excitation maxima at $<$250 nm with emission at 368 nm. This matched the C4 reported by Yamashita and colleagues (33), and C4 is thought to be a microbe-derived humic-like component. The peak of C4 at 325/396 nm (ex/em) corresponded to marine humic-like fluorescence (peak M) (34).

Compared with that of the control, the initial fluorescence intensities of the DOM addition treatments increased to different degrees, and the most enriched of the five

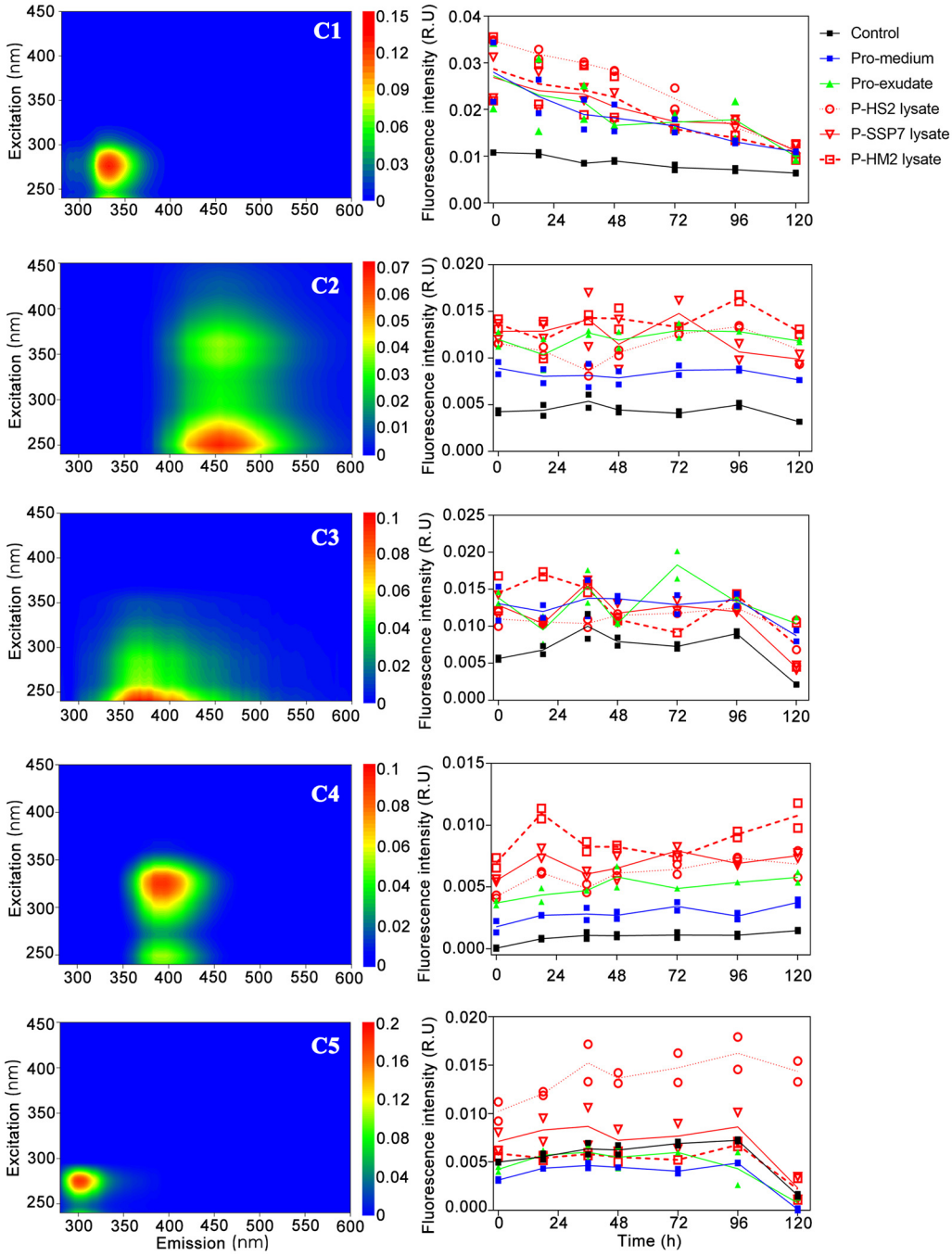

FIG 3 Microbial utilization of different components of fluorescent DOM derived from *Prochlorococcus*. Left panels, excitation-emission matrix contours of the five fluorescent components (C1 to C5) identified using PARAFAC; right panels, the corresponding FDOM component changed after incubation with different types of *Prochlorococcus*-derived DOM. The value of each replicate and the trend line of each treatment are shown.

components was C1 (Fig. S2), indicating that the DOM quality of all treatments changed after DOM addition. Since C5 contributes only a small part (10 to 20%) of the protein-like fluorescence intensity, tryptophan-like C1 was selected as representative of the protein-like components for subsequent analysis. The fluorescence intensity of C1 sharply decreased over the entire incubation period in the treatments but not in the control. After 120 h of incubation, most (50 to 70%) C1 was degraded in the Pro-medium and Pro-DOM treatments. Peaks A and C (referred to as C2 in the incubation

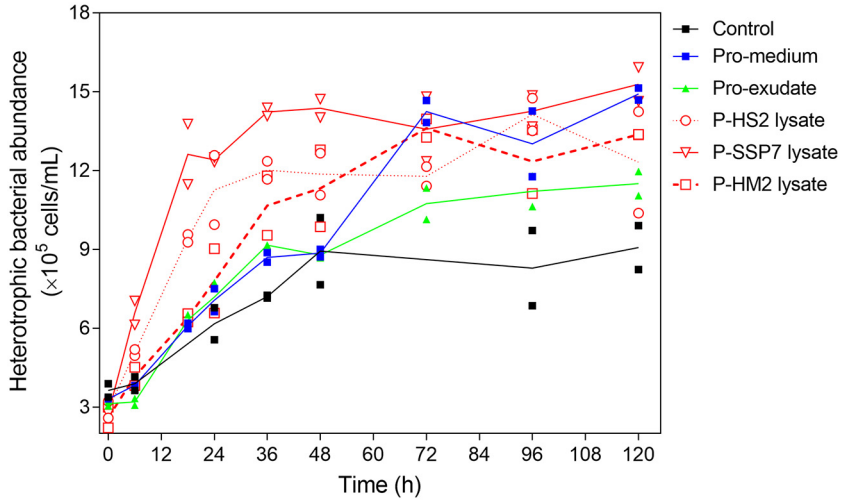

FIG 4 Growth of heterotrophic bacterioplankton after incubation with *Prochlorococcus*-derived DOM. The value of each replicate and the trend line of each treatment are shown.

experiment) showed higher fluorescence intensities for Pro-DOM than for Pro-medium (Table 1), and the intensity of C2 had different increases from 24 or 36 h of incubation for different DOM treatments (Fig. 3). These results suggest that C2 is produced not only by *Prochlorococcus* but also by heterotrophic bacteria under specific conditions. Moreover, C4 of the Pro-DOM treatment presented a higher fluorescence intensity than did that of the Pro-medium treatment and showed an intensity increase of 30 to 50%, though C4 represented only a small proportion of FDOM.

Growth of heterotrophic bacteria. During the course of the experiment, the heterotrophic bacterial abundances increased during the first phase, and later, this increase slowed and reached a stationary phase in all five treatments (Fig. 4). In the control, the bacterial abundance increased from 3.5×10^5 cells ml^{-1} at 0 h to 8.4×10^5 cells ml^{-1} at 120 h. The bacterial abundances of the five treatments increased from an average of 3.1×10^5 cells ml^{-1} at the beginning to between 12×10^5 cells ml^{-1} and 15×10^5 cells ml^{-1} at the end, with a tendency of Pro-vDOM treatments to show higher bacterial abundances than the Pro-exudate treatment.

During the incubation, the growth curves of all treatments showed log growth and a stationary phase. The bacterial specific growth (μ) of the log-growth phase was estimated by the regression slope of the natural log-transformed bacterial abundance. The μ values of the Pro-DOM and Pro-medium treatments were significantly higher than that of the control (univariate analysis of variance, $P < 0.001$), and the μ values of the P-HS2 and P-SSP7 lysate treatments were significantly higher than that of the Pro-exudate treatment (univariate analysis of variance, $P = 0.007$ and 0.016, respectively) (Table S4). Although there was no significant difference, μ of the P-HM2 lysate treatment (0.91 day^{-1}) was also higher than that of the Pro-exudate treatment (0.83 day^{-1}) (Table S4). After the stationary growth phase was reached, the bacterial abundances of all Pro-vDOM treatments were significantly higher than that of the Pro-exudate treatment (one-way analysis of variance [ANOVA], $P < 0.05$) (Table S5). Therefore, Pro-vDOM showed higher bioavailability than Pro-exudate.

Bacterial diversity and community composition. During the incubation period, the alpha diversity (Shannon and Simpson indices) of the bacterial community in the control and Pro-medium treatments remained relatively constant, whereas those of the Pro-DOM treatments decreased sharply during the first 48 h and then remained constant (Fig. S3). It was also found that the alpha diversity of Pro-vDOM was lower than that of Pro-exudate.

Alteromonadales, *Rhodospirillales*, and SAR11 accounted for more than 50% of the bacterial community throughout the experiment. The initial primary groups were

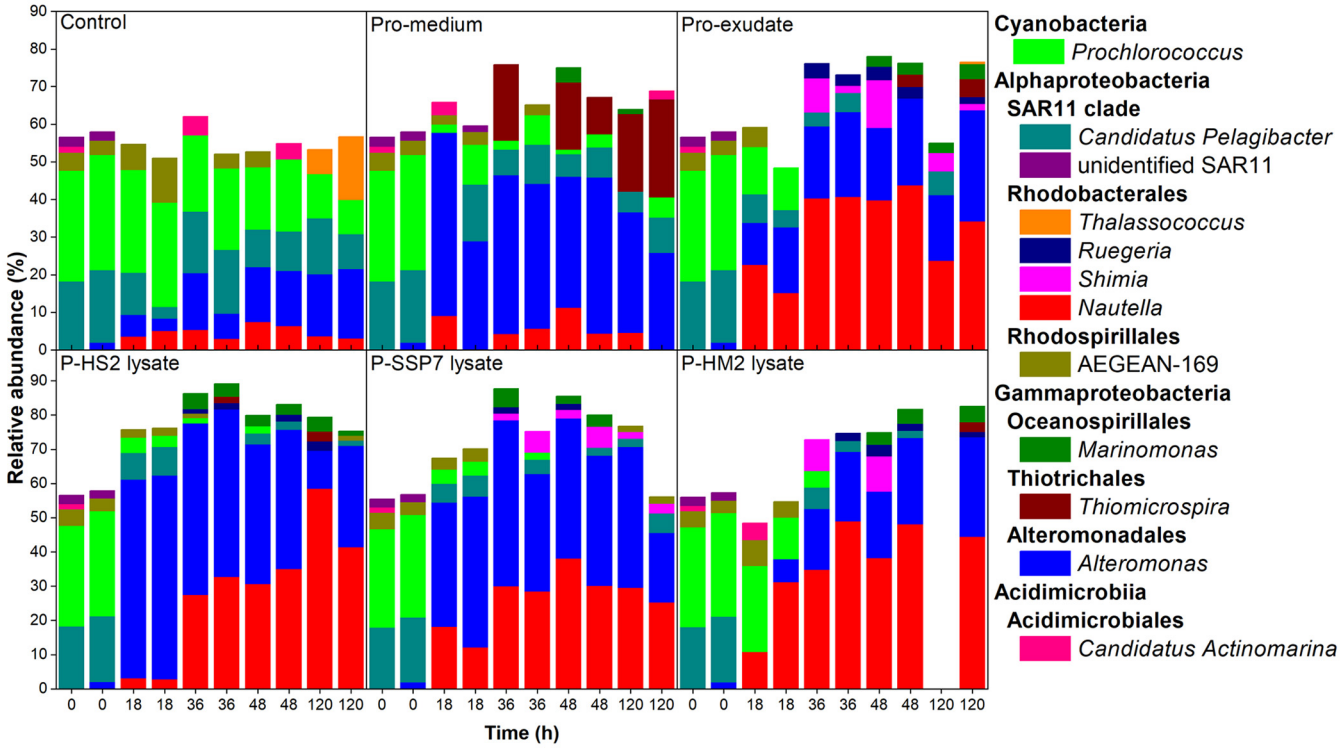

FIG 5 Response of the microbial community structure (genus level) to *Prochlorococcus*-derived DOM. The top five abundant genera in at least one sample were selected. Bars with the same number on the same graph represent replicates, and two replicates of each Pro-DOM treatment at each sampling time data are shown here (except the P-HM2 lysate at 120 h, which had only one sample). The names of the treatments are shown in the corresponding figures.

Prochlorococcus and *Pelagibacter*, and they shifted to *Nautella*, *Alteromonas*, *Prochlorococcus*, and *Pelagibacter* at the end of the experiment in the control, to *Alteromonas*, *Pelagibacter*, and *Thiomicrospira* in the Pro-medium samples, and to *Nautella* and *Alteromonas* in the Pro-DOM samples (Fig. 5). During the incubation, the relative abundances of *Rhodobacterales* and *Alteromonadales* increased, while those of the SAR11 clade and cyanobacteria decreased in all treatments. *Nautella* and *Alteromonas* were the two groups that responded quickly to Pro-DOM addition and predominated in the late period of the experiment in all DOM-amended treatments.

As shown in Fig. 6, distinct changes in the bacterial community structure mainly happened within 36 h, and then the bacterial community structure remained stable. During the experimental period, the bacterial structure of the control had a relatively small change compared with those of samples receiving DOM addition. Compared with that of the Pro-medium treatment, the bacterial community structures of Pro-DOM treatments had a distinct succession trajectory. A difference also existed between the structures of Pro-exudate and Pro-vDOM treatments (especially for the P-HS2 and P-SSP7 lysates). From 36 h, the bacterial community structures of the Pro-vDOM treatments were significantly different from that of the Pro-exudate treatment at the corresponding sampling time (SIMPROF test, $P = 0.001$), and the bacterial communities of the P-HS2 lysate and P-SSP7 lysate treatments were similar (84.6%) but significantly different from that of the Pro-exudate treatment at the 36-h and 48-h sampling points (SIMPROF test, $P = 0.001$). This indicated that the Pro-exudate and Pro-vDOM treatments have different effects on microbial community succession.

Operational taxonomic unit (OTU)-based microbial cooccurrence network analysis showed that most of the highly connected OTUs were assigned to *Alphaproteobacteria* and *Gammaproteobacteria* (Fig. 7), indicating that bacterial species in these two classes were key components of the microbial community. DOM addition significantly increased the positive interactions among microorganisms, and the graph density of the network of Pro-DOM treatments was more than two times higher than that of the

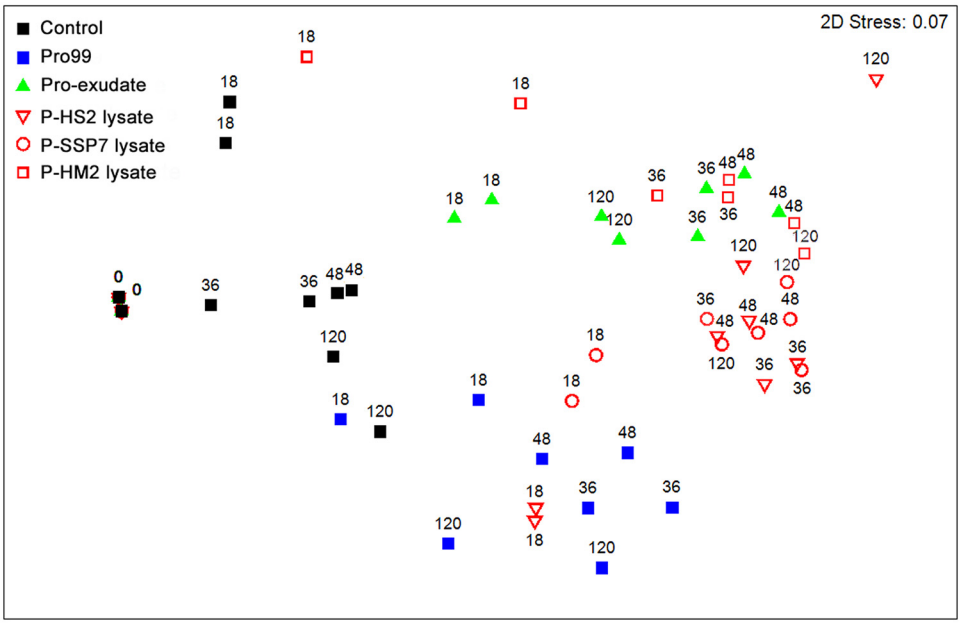

FIG 6 Effect of *Prochlorococcus*-derived DOM on the succession of the bacterial community structure, as revealed by NMDS analysis. The number on each symbol indicates the sampling time of each treatment, and all treatments at each sampling time had two replicates (except the P-HM2 lysate treatment at 120 h), as shown by two of each symbol having the same number.

control and Pro-medium treatment (Table S6). The increased interactions were due mainly to some specific OTUs that belonged to *Alphaproteobacteria* in the Pro-medium and Pro-exudate treatments and to *Alphaproteobacteria*, *Gammaproteobacteria*, and cyanobacteria in the Pro-vDOM treatments. The highly connected OTUs also differed among these DOM treatments. In the Pro-medium treatment, the OTUs belonged to the SAR11 clade and *Prochlorococcus*. *Rhodospirillaceae* and the SAR11 clade (except in the P-HM2 lysate treatment) dominated in all Pro-DOM treatments, and *Prochlorococcus* also appeared to have a close interaction with other OTUs in the Pro-vDOM treatments (except in the P-HM2 lysate treatment). The negative interactions among microorganisms were also affected by DOM addition (Table S6). There were small changes in the negative interaction in the Pro-medium and Pro-exudate treatments compared with the control. Compared with the Pro-exudate treatment, Pro-vDOM treatments had an apparent increase in negative edges and nodes with negative interactions with other nodes.

DISCUSSION

Viral lysis alters the quality of DOM released by *Prochlorococcus*. In this work, our DOC, CDOM, FDOM, and amino acid data showed that viral lysis altered the production and composition of DOM released by *Prochlorococcus*, which is the most important photosynthetic picophytoplankton in the oligotrophic ocean. This finding is consistent with those of previous studies based on other phytoplankton. Viral infection alters the lipid composition of *Emiliania huxleyi* cellular materials (9) and the composition of DOM released by *Micromonas pusilla* and *Synechococcus* (4, 13, 14). Treatments with Pro-vDOM, which contained intracellular materials of hosts, resulted in a higher a_{254}, amino acid concentration, and spectral slope $S_{275–295}$ than treatment with Pro-exudate. During the incubation, Pro-vDOM treatments resulted in a higher DOC degradation rate than the Pro-exudate treatment, and their $S_{275–295}$ values decreased more than that of the Pro-exudate treatment (Fig. 2b; see Table S3 in the supplemental material). Microbial degradation induces the decrease of $S_{275–295}$ as a result of LMW DOM consumption (35). These results suggested that more labile LMW DOM was released and then consumed in the Pro-vDOM treatments than in the Pro-exudate treatment. In

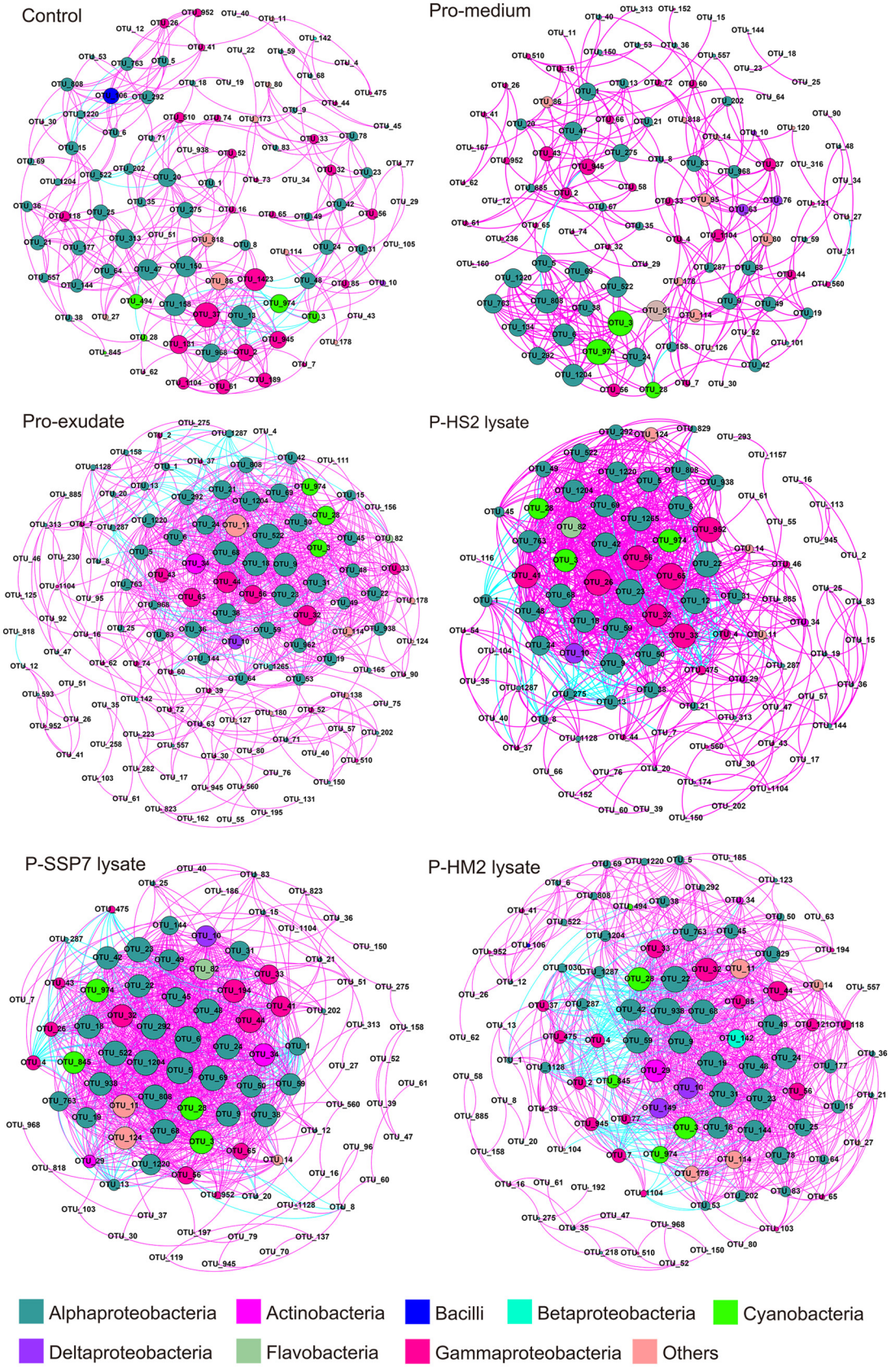

FIG 7 OTU-based network revealing intense interaction among microbial communities after incubation with *Prochlorococcus*-derived DOM. Red and cyan connections represent positive and negative interactions, respectively.

addition, the TDAA carbon yields, which indicates the degree of bioavailability of DOM (36), of the Pro-vDOM treatments were much higher than that of the Pro-exudate treatment at the beginning of incubation and close (0.8 to 1.1%) at the end of incubation (Fig. S4), resulting in the TDAA carbon yield of Pro-vDOM treatments decreasing more than that of the Pro-exudate treatment. This indicated that Pro-vDOM has higher bioavailability than Pro-exudate. This result was further supported by the finding that the heterotrophic bacterial growth rate and abundance of the Pro-vDOM treatments were significantly higher than those of the Pro-exudate treatment (Tables S4 and S5), suggesting that Pro-vDOM was easier to convert to biomass than the Pro-exudate. It is also possible that the labile DOM released by viral lysis may enhance the accessibility of RDOM to bacterial remineralization due to the priming effect (37). Therefore, the viral lysis of *Prochlorococcus* might fuel heterotrophic bacterial activity and, subsequently, the microbial loop in vast oligotrophic oceans. In the initial viral shunt concept (38), it was predicted that heterotrophic bacterial production is stimulated by viral lysis products, i.e., by organic matter that enters the DOM pool, and is hence not transferred to higher trophic levels by grazing (5). Here, we present an additional interpretation, i.e., that viral lysis not only increases the concentration of the DOM pool but also changes the quality of the DOM toward higher bioavailability.

Bacterial community fueled by different sources of DOM. Nonmetric multidimensional scaling (NMDS) analysis showed that Pro-DOM (see Materials and Methods) had significant effects on the microbial community succession trajectories (Fig. 6). Compared with the Pro-medium treatment, the Pro-DOM treatments had distinct community structures during the entire incubation period, suggesting that Pro-DOM had a significant role in shaping the microbial community. This is consistent with previously observed pronounced effects of phytoplankton-derived DOM (such as from diatoms and *Synechococcus*) on the bacterial community (39, 40). Importantly, we observed that the microbial community of the Pro-vDOM treatments had different succession trajectories than that of the Pro-exudate treatment (20). Previous works have suggested that the microbial community structure might be affected by both DOM quality and quantity (41–43). Our redundancy analysis (RDA) showed that the DOM composition could explain 50% of the total variation in the bacterial community composition, while the DOC concentration had a minor effect. This result was contrary to that reported by Sarmento and colleagues (43), who found that DOM quantity affects bacterial communities more than quality. A possible reason for this difference might be the relatively larger DOC concentration range (10, 30, and 100 μM) in their experiment than in our experiments. For example, high DOC concentrations could shift the bacterial community toward faster-growing OTUs (44). Therefore, the different responses of the microbial community structure to Pro-vDOM and Pro-exudate treatments might reflect differences in DOM quality due to providing specific ecological niches for bacteria, since similar initial DOC concentrations were used in this study.

In addition, our work showed that vDOM produced by morphologically different phages probably have diverging ecological roles, since they affected the bacterial growth rate (Fig. 4) and bacterial diversity (Fig. S3) in different ways. These differences may be related to DOM quality changes (such as the amino acid composition and concentration and protein-like FDOM production) due to variations in host-phage interactions. Thompson and colleagues demonstrated that marine cyanophages carried and expressed auxiliary metabolic genes (AMGs) and may have redirected the host carbon metabolism (45). It was reported that the three cyanophages had different burst sizes and AMGs (46), which may lead to differences in the quality of the organic matter in Pro-vDOM.

Furthermore, RDA illustrated that specific microbial taxa were linked to DOM characteristics (Fig. 8). The absorption coefficient a_{280} and protein-like FDOM C1 and C5 were positively correlated with the relative abundance of *Alteromonadales*, which was one of the dominant groups in the incubation. These results are probably explained by the fact that *Alteromonadales* was mainly responsible for CDOM removal in the dark

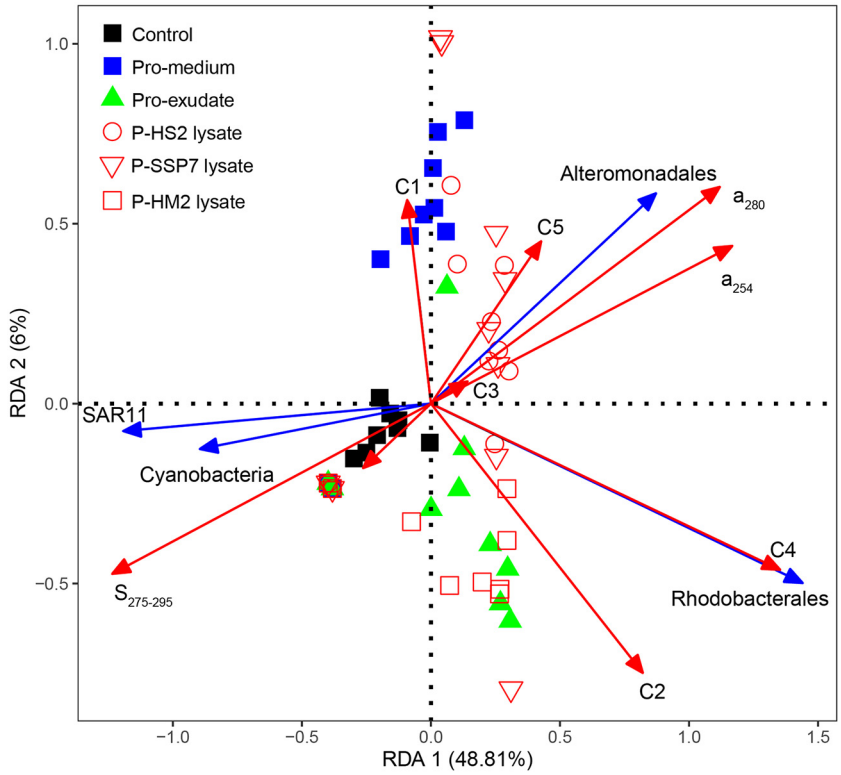

FIG 8 Redundancy analysis illustrating specific bacterial groups closely linked to specific DOM characteristics. a_{280}, C2, C5, $P = 0.001$; C4, $P = 0.01$; $S_{275-295}$, C3, $P < 0.05$; DOC, C1, a_{254}, $P > 0.05$. Only the bacterial groups that were significantly correlated with DOM indices are shown in the figure. All the bacterial community samples (without sampling times) are also presented in the figure. The samples located on the positive section of the second axis of the RDA figure are the early samples (at 18 or 36 h) of this incubation.

incubation. For C4, the humic-like FDOM component was positively related to *Rhodobacterales*, indicating that *Rhodobacterales* might be the major biological factor affecting the fate of humic-like DOM in dark conditions. Though both *Alteromonadales* and *Rhodobacterales* were the dominant groups in this experiment, the major roles of the two may differ in carbon processing. *Alteromonadales* have a broad substrate preference relative to that of *Rhodobacterales* (47–49) and may apply diverse complementary growth strategies to rapidly respond to external disturbances. The coefficients a_{280}, C1, and C5 closely correlated with early samples (in 18 h), and C4 was correlated with later samples. This indicates that the early period was the DOM removal and biomass accumulation phase and that the late phase was responsible for humic-like DOM accumulation. This is supported by previous works showing that bacteria incorporate labile DOM into biomass but respire low-quality DOM and produce humic-like by-products (50, 51).

In microbial cooccurrence network analysis, positive relationships indicate cooperation, cocolonization, or niche overlap while negative relationships suggest competition or a prey-predator relationship (52). Compared with the control and the Pro-medium treatment, Pro-DOM addition significantly increased the positive relationship among microorganisms (Table S6). The possible reason was that Pro-DOM is a complex DOM mixture and needs additional microbial cooperation to be utilized. Furthermore, the average degree of the network of Pro-vDOM was higher than that of Pro-exudate (Table S6), indicating that denser interactions among species appeared in the Pro-vDOM treatments than in the Pro-exudate treatment. In addition, negative interactions increased in the Pro-vDOM treatments but not in the Pro-exudate treatment. Detailed

analysis showed that the negative interactions happened mainly between the high-relative-abundance OTUs (*Nautella*, *Alteromonas*, *Marinomonas*) and other OTUs. These results suggested that these bacteria may have a greater competitive pressure in Pro-vDOM treatments than in the Pro-exudate treatment, indicating that Pro-vDOM is likely more labile to oligotrophic microorganisms than Pro-exudate.

Implication: the impact of viral lysis on the production and transformation of DOM in the ocean. Peak M represents the primary humic-like material in *Prochlorococcus*-derived FDOM (Table 1), which is thought to be autochthonous humic-like DOM in the global ocean with a ubiquitously distributed microbial origin (32). The relatively high peak-M fluorescence intensity of the Pro-vDOM treatments indicated that viral lysis is a pathway that contributes considerably to the release of humic-like materials produced by *Prochlorococcus*. Previous global and regional surveys show that chlorophyll *a* is closely related to the distribution of peak M in oligotrophic epipelagic oceans (30, 53), where *Prochlorococcus* is the numerically dominant phytoplankton (22). In addition, *Prochlorococcus* has a vertical distribution pattern similar to that of peak M in the open ocean (30, 54). This indicates that viral lysis of *Prochlorococcus* is an important humic-like DOM source in the ocean. Considering the wide distribution and long turnover times (610 years) of peak M in the ocean (55), viral lysis of *Prochlorococcus* contributes to the recalcitrant DOM pool in the water column through microbial carbon pump (17).

Our study with isolates demonstrates that viral lysis is a source of labile and humic-like substances. It has been reported that cyanophage infection redirects host metabolism (45, 56), and it has been proposed that phage-encoded AMGs are responsible for this reprogramming (57). This suggests that viral infection plays a vital role in affecting the host metabolism and the quality of host-released DOM and might have contributed to our findings. Moreover, virus-induced mortality contributes significantly to marine phytoplankton losses (5, 7). Therefore, we hypothesize that viral lysis is also a potentially important source of labile and humic-like material in the global ocean (4, 16).

Methodological limitations. Microcosm incubation is one of the approaches widely used to assess the availability of DOM for natural microorganisms (12, 43, 58). In our experimental setup, to eliminate grazing in the incubation, 0.8-μm filtration was used to remove predators such as heterotrophic nanoflagellates and particles (12, 39, 59). Previous studies showed that 1- or 0.8-μm filtration can eliminate all heterotrophic nanoflagellates in most coastal and open regions of the South China Sea and the Atlantic Ocean (60, 61). However, the filtration inevitably results in a certain loss of bacterial cells and the alteration of bacterial growth. To minimize these effects as much as possible, we used a low filtration pressure and polycarbonate membranes instead of glass fiber membranes, which can reduce the effect of filtration on the selective loss of bacteria (62).

During *Prochlorococcus* DOM preparation, we used a standard culture medium, Pro99 (63), to culture *Prochlorococcus* under continuous-light conditions for a better cell yields. It is worth pointing out that the nutrient concentrations (N/P) of Pro99 medium were higher than those in natural seawater (see reference 63 and references therein). So far, there is no evidence indicating that the physiological and ecological characteristics of *Prochlorococcus* grown in Pro99 medium are different from those *in situ*. For example, their temperature optima and light requirements are consistent with their distribution in the ocean (54). However, it is unknown whether the modification of these culture conditions affects the composition of *Prochlorococcus* DOM released during viral infection. In addition, in accordance with previous studies (39, 47, 58), the present study added a relatively lower percentage of DOC into the incubation systems compared with environmental conditions. However, the DOM amendments should be higher than the amount of DOC released by *Prochlorococcus* in *in situ* environments. Based on the available data regarding the *Prochlorococcus* viral mortality rate (8, 24, 25), cellular carbon content (64), and DOC exuded rate (3), it is estimated that *Prochlorococcus* contributed DOC of less than 1 μmol C liter^{-1} day^{-1} under *in situ*

conditions. Therefore, the addition of DOM may impact, and will probably stimulate, bacterial growth. The possible differences in quantity and quality of the *Prochlorococcus* DOM between our microcosm and natural environments need to be considered when applying our conclusions to biogeochemical studies. Moreover, viral lysis contributes to the production of both dissolved and particulate (cell debris) organic matter. Most studies, including the present one, have focused on DOM (12, 16, 21). To obtain a complete view of virus-driven production and transformation of organic matter, more investigations on organic particles generated during lysis are needed.

Conclusions. In summary, we demonstrated that viral lysis altered the quality and quantity of DOM released by *Prochlorococcus*, and hence, viral lysates of *Prochlorococcus* might be a pathway that considerably contributes to marine CDOM and humic-like DOM pools. These results are an important step toward linking laboratory studies and large-scale oceanographic surveys by potentially allowing identification of sources of vDOM in the ocean. *Prochlorococcus* lysates were more labile than the *Prochlorococcus* exudate and shaped the microbial community with different succession trajectories. Under the conditions of global climate change, the distribution of *Prochlorococcus* might broaden, its abundance might increase (22), and the contribution of viral lysis to phytoplankton mortality might be enhanced (8). The data suggest that viral infection of *Prochlorococcus* may play an important role in shaping DOM cycling and pooling in oligotrophic oceans.

MATERIALS AND METHODS

***Prochlorococcus* DOM collection.** *Prochlorococcus* MED4 and three phages with different morphologies (myovirus P-HM2, siphovirus P-HS2, and podovirus P-SSP7) used in this work are routinely maintained at The Hong Kong University of Science and Technology (see Table S1 in the supplemental material). Axenic *Prochlorococcus* strain MED4 was cultivated in eight 1-liter polycarbonate bottles in Port Shelter (Hong Kong) seawater-based Pro99 medium (Pro-medium, 800 ml) with 50 μM $NaHPO_4$, 800 μM NH_4Cl, and trace metal mix (63) at 23°C under constant cool white light (30 microeinsteins m^{-2} s^{-1}) (the method used for the axenicity tests for *Prochlorococcus* is shown in the supplemental methods). After reaching the early-logarithmic growth phase (an abundance of ca. 10^8 cells ml^{-1}), six cultures were inoculated with myovirus P-HM2, siphovirus P-HS2, and podovirus P-SSP7 (ca. 10^9 particles ml^{-1}) at a ratio of 1:100 (vol/vol; corresponding multiplicity of infection [MOI] of 0.1) . One week later, the cultures were filtered through 0.2-μm polycarbonate membranes (47 mm; Millipore, USA). All filtrates and 2 liters of Pro-medium were stored in precombusted (450°C for 6 h) 450-ml Boston round amber glass bottles (CNW, Germany) at 4°C and used within 3 weeks. All filtration procedures were conducted at low pressure in a clean-hand bench. Here, we define P-HS2, P-HM2, and P-SSP7 lysates as virus-derived DOM (Pro-vDOM), the filtrate of *Prochlorococcus* culture without virus addition as Pro-exudate, Pro99 medium as Pro-medium, and Pro-DOM as including both Pro-exudate and Pro-vDOM.

Before performance of dark incubation experiments, the DOC, CDOM, FDOM, and amino acids of the obtained DOM (Pro-DOM and Pro-medium) were measured (see below).

Dark incubation experiments. To examine the biodegradability of different DOMs derived from *Prochlorococcus* and the response of the oligotrophic bacterial community to these DOM, Pro-exudate and Pro-vDOM were added to and incubated with oligotrophic seawater (Fig. S1). The surface water was collected from the SEATS station (a well-investigated oligotrophic station) (65) at a 5-m depth in the South China Sea, using a rosette sampler with a conductivity-temperature-depth instrument, which yielded a recorded temperature of 29.5°C and a salinity of 33.3, on 6 November 2016. The seawater was filtered through a 0.8-μm-pore-size membrane (the filter sets were prewashed with 20 liters of ultrapure Milli-Q water, and the first 10 liters of seawater filtrate was discarded) to eliminate predators and particles intermediately and then dispatched into 12 10-liter acid-prewashed polycarbonate carboys (wrapped with foil). The filtered seawater was amended with the following DOM sources: Pro-medium, Pro-exudate, and three *Prochlorococcus* virus lysates (namely, P-HS2 lysate, P-SSP7 lysate, and P-HM2 lysate). Studies have revealed that both DOM quality and quantity influence the microbial community (41, 42). A recent study showed that DOM quantity affects the bacterial community more than quality does (43). In this study, we added a low dose of DOM (8 to 15 μM) into each microcosm to avoid "shock" from DOM addition to microbial communities and to simulate the *in situ* conditions of the oligotrophic open ocean. Each DOM treatment had two replicates. Another two carboys contained an 0.8-μm-filtered seawater sample without any treatment and were used as the controls for this experiment. During the experiment duration, samples were collected to determine the DOC concentration, CDOM, FDOM, amino acid, prokaryotic abundance, and bacterial community.

DOC analysis. Dissolved organic carbon (DOC) samples were collected at 0, 6, 18, 36, 48, and 120 h with precombusted (450°C, 6 h) glass pipettes and stored in precombusted (450°C, 6 h) 40-ml amber vials at −20°C until further analysis. Three subsamples were collected from each replicate. In this study, the incubation used 0.8-μm-filtered seawater, and the total organic carbon concentration was

equivalent to the DOC concentration. Before analysis, the samples were thawed at room temperature and then acidified to pH <2. The DOC concentration was measured using the high-temperature combustion method on a Shimadzu TOC-VCPH organic carbon analyzer. Three to five injections of 150 μl were performed per sample until the coefficient of variation on the analysis of replicate measurements was approximately 2%. The concentrations were determined by subtracting the values from a blank of ultrapure Milli-Q water and dividing the result by the slope of a daily standard curve made from potassium hydrogen phthalate. All samples were checked against deep-sea reference water and low-carbon water (provided by the Hansell Organic Biogeochemistry Laboratory, University of Miami, USA). The analytical precision was $\pm$1.7 μmol C liter^{-1} as indicated by the standard deviation of DOC measurement of deep-sea reference water ($n = 18$).

Total amino acid analysis. Samples for total dissolved amino acid (TDAA) analysis were directly collected from the carboys with precombusted (450°C, 6 h) glass pipettes and stored in 40-ml precombusted (450°C, 6 h) amber glass vials at −20°C until analysis. The measurement of TDAA used a previously established method (66), and the detailed method and settings were as described by Li and colleagues (67). Thirteen amino acids, namely, aspartic acid (Asp), glutamic acid (Glu), serine (Ser), arginine (Arg), glycine (Gly), threonine (Thr), alanine (Ala), tyrosine (Tyr), valine (Val), phenylalanine (Phe), isoleucine (Ile), leucine (Leu), and γ-aminobutyric acid (GABA) were measured.

A 2-ml subsample was added to a screw-top tube spiked with 2 ml concentrated HCl (trace metal grade; Fisher, USA) and sealed under nitrogen before being hydrolyzed at 110°C for 24 h. The hydrolyzed samples were dried with ultrapure nitrogen gas, dissolved in ultrapure Milli-Q water, and finally spiked with aminoadipic acid. Then, 1 ml of the obtained sample was transferred to a 2-ml vial and then reacted with 100 μl of an *o*-phthaldialdehyde (OPA) solution at room temperature for 2 min. A 20-μl aliquot was injected into a high-performance liquid chromatography (HPLC) system coupled with a fluorescence detector (Shimadzu RF-20A) with excitation and emission wavelengths of 330 nm and 418 nm, respectively. The separation of amino acids was accomplished using a reverse-phase C_{18} column (InertSustain; 250 by 4.6 mm, particle size of 5 μm) at a flow rate of 1.0 ml min^{-1}. Mobile phase A consisted of 0.04 M potassium phosphate monobasic buffer with 1% tetrahydrofuran, and the pH was adjusted to 6.2 with potassium hydroxide. Mobile phase B consisted of HPLC-grade methanol, acetonitrile, and ultra-pure water mixed at a volume ratio of 4.5:4.5:1. The elution gradient (67) was performed over 73 min. The relative standard deviation of triplicate analyses was $<$3%. Ultrapure Milli-Q water was used as the blank for every measurement batch. The mean peak areas of each amino acid in the blanks were subtracted from the corresponding peaks of all samples. The blanks were generally less than 2% of the sample signals measured in this research.

CDOM absorption, EEM measurement, and parallel factor analysis modeling. CDOM and FDOM sampling were performed at 0, 18, 36, 48, 72, 96, and 120 h. All CDOM and FDOM samples were kept frozen (–20°C) until further analysis. Storing CDOM samples at −20°C is a commonly used method for CDOM analyses, and a number of marine DOM studies show the minimal effects from freezing/thawing on DOM optical properties (68, 69). Ultrapure Milli-Q water was used as the absorbance and fluorescence blank. DOM absorption was measured as previously described (70). Namely, the absorption scans ranged from 240 to 800 nm at 1-nm intervals using a 2300 UV-visible spectrophotometer (Techcomp, China) with a 10-cm-path-length quartz cell at constant room temperature. Ultrapure water was measured every three samples to detect and adjust for possible instrument drift. After subtraction of the average absorbance value between 700 nm and 750 nm, absorbance values were converted to Napierian absorption coefficients using the following equation: $a = 2.303A/L$, where a is the Napierian absorption coefficient (m^{-1}), A is the absorbance measured by the spectrophotometer, and L is the path length (m). The spectral slope over the wavelength range from 275 to 295 nm ($S_{275–295}$) was calculated by linear regression of natural log-transformed absorption spectra (35). Helms and colleagues (35) demonstrated that the $S_{275–295}$ can be related to the relative molecular weight of DOM, and high $S_{275–295}$ values typically indicate LMW DOM.

Fluorescence measurements were analyzed as previously described (70). Briefly, EEMs were obtained using a Cary Eclipse (Varian, Australia) fluorimeter equipped with a 150-W Xe arc lamp. The configuration included excitation from 250 to 450 nm in 5-nm intervals, with acquisition from 280 to 600 nm at 2-nm intervals and 10-nm and 5-nm slit widths on the excitation and emission modes, respectively. The scan speed was 1,920 nm min^{-1}, with the photomultiplier voltage set to 800 V. The EEMs of the samples were blank corrected and Raman normalized using ultrapure Milli-Q water EEMs scanned on the same day. In total, 168 EEM spectra were modeled using PARAFAC with MATLAB 7.5 and the DOMFluor toolbox (71). Split-half validation was used to determine the number of fluorescent components. The fluorescence intensity of each fluorescent component was evaluated using the maximum fluorescence. EEM maps of *Prochlorococcus*-derived DOM were obtained after subtraction of the blank and normalization to the ultrapure Milli-Q water Raman peak scanned on the same day. The fluorescent components of the obtained *Prochlorococcus*-derived DOM stocks were obtained by the traditional "peak-picking" method (32).

Prokaryotic abundance analysis. The prokaryotic abundance was determined at 0, 6, 12, 18, 24, 36, 48, 72, 96, and 120 h by the established methods (72). At each sampling time, 1.8-ml subsamples were fixed with a final concentration of 0.5% glutaraldehyde for 15 min in the dark, flash-frozen in liquid nitrogen, and stored at −80°C until analysis. Before analysis, the frozen prokaryotic abundance samples were thawed in a 37°C bath. Then, 990-μl samples were stained with 10 μl SYBR green I (Sigma-Aldrich, St. Louis, MO) for 15 min in the dark, and 10 μl 1-μm calibration beads (BD Bioscience) were added as a reference before counting by flow cytometer (BD Accuri C6, USA), and prokaryotes were identified in plots of red fluorescence versus green fluorescence. Autotrophic picoplankton abundance was analyzed

on a BD FACSAria flow cytometer, and 1-μm calibration beads were used for the flow rate calibration; autotrophic picoplankton are identified in plots of side scatter versus red fluorescence. Heterotrophic bacterial abundance was obtained by subtracting autotrophic cell abundance from prokaryotic abundance. The flow cytometric data were analyzed with the BD Accuri C6 software and FCS Express software.

DNA extraction, sequencing, and analysis. One liter of seawater from each treatment was collected at 0, 18, 36, 48, and 120 h and filtered through 0.2-μm polycarbonate filters (Millipore; 47-mm diameter) under low pressure (less than 30 kPa), and the filters were stored at −80°C until further analysis. Note that samples at 0 h were collected only from the control, and all the treatments shared the initial bacterial community structure of these samples. DNA was extracted from the samples by use of a previously described method (73).

The 16S rRNA gene V3-V4 region was amplified using a specific primer pair (341F-806R) (74) with a barcode. All PCRs were carried out with Phusion high-fidelity PCR master mix (New England Biolabs). Samples with bright main bands between 450 and 550 bp were chosen, and the band contents were purified with a Qiagen gel extraction kit (Qiagen, Germany). The amplicons were paired-end sequenced using the HiSeq2500 platform (Illumina, Inc., San Diego, CA, USA). Sequences were assigned to each sample based on the barcode and truncated by cutting off the barcode and primer sequence. Sequence assembly was conducted with FLASH (v1.2.7) (75), and low-quality sequences were filtered under specific filtering conditions according to the QIIME (v1.7.0) quality control process (76). Chimeric sequences were detected with the Genomes Online Database (GOLD) using the UCHIME algorithm and then removed (77). Effective tags were then finally obtained.

Sequence analysis was performed by UPARSE software (UPARSE v7.0.1001) (78). Sequences were assigned to the same OTUs at 97% similarity, and a representative sequence for each OTU was screened for further annotation. The OTU taxonomic information was annotated using the RDP classifier (version 2.2) (79) with the Greengenes database (80). The OTU abundance was normalized using a standard sequence number corresponding to the sample containing the fewest sequences. Subsequent analyses of alpha diversity and beta diversity were performed based on this output-normalized data.

Microbial network analysis. A network was constructed by following a previously published method (81), with some modification. OTUs were defined at 97% similarity, and those with a relative abundance above 0.1% in one sample that appeared in more than two samples of all treatments were selected. We calculated all possible Spearman's rank correlations between these OTUs. We considered a valid cooccurrence event to be a robust correlation if the Spearman's correlation coefficient was >0.6 and a statistically significant P value of <0.01 was present. The networks of each treatment were displayed separately with Gephi 0.9.2. To describe the topology of the network, some basic indices (node, edge, average degree, graph density, and others) were calculated.

Statistical analysis. Statistical analyses, including t tests to examine the differences in the optical parameters of the generated DOM between Pro-exudate and Pro-vDOM, one-way ANOVAs to compare the differences in the heterotrophic bacterial abundance and DOM utilization rate, the calculation of the specific growth rate (μ) according to the general linear regression slope between the log-transformed bacterial abundance and growth time, and univariate analysis to test the differences between the resulting μ values, were performed using IBM SPSS Statistics 25.0 (IBM Corp., USA).

NMDS analysis for the bacterial community structure and the SIMPROF test for bacterial community similarity were performed with Primer 6 (PRIMER-E, United Kingdom). Bacterial relative abundance data were not transformed during NMDS and SIMPROF analysis. The R package (version 3.4.3) was used for the RDA. Before RDA, bacterial relative abundance data were transformed by Hellinger transformation, environmental factor (DOC, $S_{275–295}$, a_{280}, a_{254}, C1, C2, C3, C4, and C5) data were zero centered and normalized, and covariabilities among environmental factors were examined using variance inflation factors (factors of less than 10 were selected). RDA was conducted with the vegan package via the permutation test (999 permutations).

Data availability. The sequences reported in this paper have been deposited in the National Center for Biotechnology Information database under BioProject no. PRJNA644149 (released 7 November 2020).

SUPPLEMENTAL MATERIAL

Supplemental material is available online only.

SUPPLEMENTAL FILE 1, PDF file, 1.2 MB.

ACKNOWLEDGMENTS

This work was supported by National Natural Science Foundation of China projects (grant no. 41861144018 to N. Jiao, 91951209 to R. Zhang, 41876083 to W. Guo, and 41676059 and 41890801 to X. Li), by the Research Grants Council of the Hong Kong Special Administrative Region, China (grant no. 16102317), to Q. Zeng, and by the Programme of Introducing Talents of Discipline to Universities (BP0719030) to M. G. Weinbauer.

We thank the captain, crew, and scientists aboard the *R/V Shiyan III*, led by chief scientist Jia Sun, for their support during the cruise. We thank Qiaoyun Qin for assistance in using R software (RDA) and Adobe Illustrator (Fig. S1), Jing Xu for technical

support during FDOM data analysis, and three anonymous reviewers whose comments improved the manuscript.

We declare no competing interests.

REFERENCES

1. Field CB, Behrenfeld MJ, Randerson JT, Falkowski P. 1998. Primary production of the biosphere: integrating terrestrial and oceanic components. Science 281:237–240. https://doi.org/10.1126/science.281.5374.237.
2. Falkowski PG, Raven JA. 2007. Aquatic photosynthesis in biogeochemical cycles, p 364–410. *In* Falkowski PG, Raven JA (ed), Aquatic photosynthesis, 2nd ed. Princeton University Press, Princeton, NJ.
3. Bertilsson S, Berglund O, Pullin MJ, Chisholm SW. 2005. Release of dissolved organic matter by Prochlorococcus. Vie Et Milieu-Life and Environment 55:225–231.
4. Lønborg C, Middelboe M, Brussaard CPD. 2013. Viral lysis of Micromonas pusilla: impacts on dissolved organic matter production and composition. Biogeochemistry 116:231–240. https://doi.org/10.1007/s10533-013-9853-1.
5. Fuhrman JA. 1999. Marine viruses and their biogeochemical and ecological effects. Nature 399:541–548. https://doi.org/10.1038/21119.
6. Thornton DCO. 2014. Dissolved organic matter (DOM) release by phytoplankton in the contemporary and future ocean. Eur J Phycol 49:20–46. https://doi.org/10.1080/09670262.2013.875596.
7. Suttle CA, Chan AM, Cottrell MT. 1990. Infection of phytoplankton by viruses and reduction of primary productivity. Nature 347:467–469. https://doi.org/10.1038/347467a0.
8. Mojica KDA, Huisman J, Wilhelm SW, Brussaard CPD. 2016. Latitudinal variation in virus-induced mortality of phytoplankton across the North Atlantic Ocean. ISME J 10:500–513. https://doi.org/10.1038/ismej.2015.130.
9. Evans C, Pond DW, Wilson WH. 2009. Changes in Emiliania huxleyi fatty acid profiles during infection with E. huxleyi virus 86: physiological and ecological implications. Aquat Microb Ecol 55:219–228. https://doi.org/10.3354/ame01295.
10. Chrost RH, Faust MA. 1983. Organic carbon release by phytoplankton: its composition and utilization by bacterioplankton. J Plankton Res 5:477–493. https://doi.org/10.1093/plankt/5.4.477.
11. Chen W, Wangersky PJ. 1996. Rates of microbial degradation of dissolved organic carbon from phytoplankton cultures. J Plankton Res 18:1521–1533. https://doi.org/10.1093/plankt/18.9.1521.
12. Zhao Z, Gonsior M, Schmitt-Kopplin P, Zhan Y, Zhang R, Jiao N, Chen F. 2019. Microbial transformation of virus-induced dissolved organic matter from picocyanobacteria: coupling of bacterial diversity and DOM chemodiversity. ISME J 13:2551–2565. https://doi.org/10.1038/s41396-019-0449-1.
13. Ma XF, Coleman ML, Waldbauer JR. 2018. Distinct molecular signatures in dissolved organic matter produced by viral lysis of marine cyanobacteria. Environ Microbiol 20:3001–3011. https://doi.org/10.1111/1462-2920.14338.
14. Zhao Z, Gonsior M, Luek J, Timko S, Ianiri H, Hertkorn N, Schmitt-Kopplin P, Fang XT, Zeng QL, Jiao NZ, Chen F. 2017. Picocyanobacteria and deep-ocean fluorescent dissolved organic matter share similar optical properties. Nat Commun 8:15284. https://doi.org/10.1038/ncomms15284.
15. Fiore CL, Longnecker K, Soule MCK, Kujawinski EB. 2015. Release of ecologically relevant metabolites by the cyanobacterium *Synechococcus* elongatus CCMP 1631. Environ Microbiol 17:3949–3963. https://doi.org/10.1111/1462-2920.12899.
16. Gobler CJ, Hutchins DA, Fisher NS, Cosper EM, Sanõudo-Wilhelmy SA. 1997. Release and bioavailability of C, N, P, Se, and Fe following viral lysis of a marine chrysophyte. Limnol Oceanogr 42:1492–1504. https://doi.org/10.4319/lo.1997.42.7.1492.
17. Jiao N, Herndl GJ, Hansell DA, Benner R, Kattner G, Wilhelm SW, Kirchman DL, Weinbauer MG, Luo TW, Chen F, Azam F. 2010. Microbial production of recalcitrant dissolved organic matter: long-term carbon storage in the global ocean. Nat Rev Microbiol 8:593–599. https://doi.org/10.1038/nrmicro2386.
18. Azam F, Fenchel T, Field JG, Gray JS, Meyer-Reil LA, Thingstad F. 1983. The ecological role of water-column microbes in the sea. Mar Ecol Prog Ser 10:257–263. https://doi.org/10.3354/meps010257.
19. Haaber J, Middelboe M. 2009. Viral lysis of Phaeocystis pouchetii: implications for algal population dynamics and heterotrophic C, N and P cycling. ISME J 3:430–441. https://doi.org/10.1038/ismej.2008.125.
20. Sheik AR, Brussaard CPD, Lavik G, Lam P, Musat N, Krupke A, Littmann S, Strous M, Kuypers MMM. 2014. Responses of the coastal bacterial community to viral infection of the algae Phaeocystis globosa. ISME J 8:212–225. https://doi.org/10.1038/ismej.2013.135.
21. Fang X, Liu Y, Zhao Y, Chen Y, Liu R, Qin Q-L, Li G, Zhang Y-Z, Chan W, Hess WR, Zeng Q. 2019. Transcriptomic responses of the marine cyanobacterium Prochlorococcus to viral lysis products. Environ Microbiol 21:2015–2028. https://doi.org/10.1111/1462-2920.14513.
22. Flombaum P, Gallegos JL, Gordillo RA, Rincon J, Zabala LL, Jiao NAZ, Karl DM, Li WKW, Lomas MW, Veneziano D, Vera CS, Vrugt JA, Martiny AC. 2013. Present and future global distributions of the marine Cyanobacteria Prochlorococcus and Synechococcus. Proc Natl Acad Sci U S A 110:9824–9829. https://doi.org/10.1073/pnas.1307701110.
23. Partensky F, Garczarek L. 2010. Prochlorococcus: advantages and limits of minimalism. Annu Rev Mar Sci 2:305–331. https://doi.org/10.1146/annurev-marine-120308-081034.
24. Pasulka AL, Samo TJ, Landry MR. 2015. Grazer and viral impacts on microbial growth and mortality in the southern California Current Ecosystem. J Plankton Res 37:320–336. https://doi.org/10.1093/plankt/fbv011.
25. Baudoux AC, Veldhuis MJW, Witte HJ, Brussaard CPD. 2007. Viruses as mortality agents of picophytoplankton in the deep chlorophyll maximum layer during IRONAGES III. Limnol Oceanogr 52:2519–2529. https://doi.org/10.4319/lo.2007.52.6.2519.
26. Lea-Smith DJ, Biller SJ, Davey MP, Cotton CAR, Sepulveda BMP, Turchyn AV, Scanlan DJ, Smith AG, Chisholm SW, Howe CJ. 2015. Contribution of cyanobacterial alkane production to the ocean hydrocarbon cycle. Proc Natl Acad Sci U S A 112:13591–13596. https://doi.org/10.1073/pnas.1507274112.
27. Becker JW, Berube PM, Follett CL, Waterbury JB, Chisholm SW, DeLong EF, Repeta DJ. 2014. Closely related phytoplankton species produce similar suites of dissolved organic matter. Front Microbiol 5:111. https://doi.org/10.3389/fmicb.2014.00111.
28. Bouman HA, Ulloa O, Scanlan DJ, Zwirglmaier K, Li WKW, Platt T, Stuart V, Barlow R, Leth O, Clementson L, Lutz V, Fukasawa M, Watanabe S, Sathyendranath S. 2006. Oceanographic basis of the global surface distribution of Prochlorococcus ecotypes. Science 312:918–921. https://doi.org/10.1126/science.1122692.
29. Hansen AM, Kraus TEC, Pellerin BA, Fleck JA, Downing BD, Bergamaschi BA. 2016. Optical properties of dissolved organic matter (DOM): effects of biological and photolytic degradation. Limnol Oceanogr 61:1015–1032. https://doi.org/10.1002/lno.10270.
30. Catalá TS, Álvarez-Salgado XA, Otero J, Iuculano F, Companys B, Horstkotte B, Romera-Castillo C, Nieto-Cid M, Latasa M, Morán XAG, Gasol JM, Marrasé C, Stedmon CA, Reche I. 2016. Drivers of fluorescent dissolved organic matter in the global epipelagic ocean. Limnol Oceanogr 61:1101–1119. https://doi.org/10.1002/lno.10281.
31. Yamashita Y, Tanoue E. 2008. Production of bio-refractory fluorescent dissolved organic matter in the ocean interior. Nat Geosci 1:579–582. https://doi.org/10.1038/ngeo279.
32. Coble PG. 1996. Characterization of marine and terrestrial DOM in seawater using excitation emission matrix spectroscopy. Mar Chem 51:325–346. https://doi.org/10.1016/0304-4203(95)00062-3.
33. Yamashita Y, Panton A, Mahaffey C, Jaffé R. 2011. Assessing the spatial and temporal variability of dissolved organic matter in Liverpool Bay using excitation-emission matrix fluorescence and parallel factor analysis. Ocean Dynamics 61:569–579. https://doi.org/10.1007/s10236-010-0365-4.
34. Kothawala DN, von Wachenfeldt E, Koehler B, Tranvik LJ. 2012. Selective loss and preservation of lake water dissolved organic matter fluorescence during long-term dark incubations. Sci Total Environ 433:238–246. https://doi.org/10.1016/j.scitotenv.2012.06.029.
35. Helms JR, Stubbins A, Ritchie JD, Minor EC, Kieber DJ, Mopper K. 2008. Absorption spectral slopes and slope ratios as indicators of molecular weight, source, and photobleaching of chromophoric dissolved organic matter. Limnol Oceanogr 53:955–969. https://doi.org/10.4319/lo.2008.53.3.0955.
36. Shen Y, Fichot CG, Benner R. 2012. Dissolved organic matter composition and bioavailability reflect ecosystem productivity in the Western Arctic

Ocean. Biogeosciences 9:4993–5005. https://doi.org/10.5194/bg-9-4993-2012.
37. Bianchi TS, Thornton DCO, Yvon-Lewis SA, King GM, Eglinton TI, Shields MR, Ward ND, Curtis J. 2015. Positive priming of terrestrially derived dissolved organic matter in a freshwater microcosm system. Geophys Res Lett 42:5460–5467. https://doi.org/10.1002/2015GL064765.
38. Wilhelm SW, Suttle CA. 1999. Viruses and nutrient cycles in the sea—viruses play critical roles in the structure and function of aquatic food webs. Bioscience 49:781–788. https://doi.org/10.2307/1313569.
39. Landa M, Blain S, Harmand J, Monchy S, Rapaport A, Obernosterer I. 2018. Major changes in the composition of a Southern Ocean bacterial community in response to diatom-derived dissolved organic matter. FEMS Microbiol Ecol 94:fiy034. https://doi.org/10.1093/femsec/fiy034.
40. Tada Y, Suzuki K. 2016. Changes in the community structure of free-living heterotrophic bacteria in the open tropical Pacific Ocean in response to microalgal lysate-derived dissolved organic matter. FEMS Microbiol Ecol 92:fiw099. https://doi.org/10.1093/femsec/fiw099.
41. Docherty KM, Young KC, Maurice PA, Bridgham SD. 2006. Dissolved organic matter concentration and quality influences upon structure and function of freshwater microbial communities. Microb Ecol 52:378–388. https://doi.org/10.1007/s00248-006-9089-x.
42. Logue JB, Lindström ES. 2008. Biogeography of bacterioplankton in inland waters. Freshwater Rev 1:99–114. https://doi.org/10.1608/FRJ-1.1.9.
43. Sarmento H, Morana C, Gasol JM. 2016. Bacterioplankton niche partitioning in the use of phytoplankton-derived dissolved organic carbon: quantity is more important than quality. ISME J 10:2582–2592. https://doi.org/10.1038/ismej.2016.66.
44. Zhang R, Weinbauer M, Tam Y, Qian P-Y. 2013. Response of bacterioplankton to a glucose gradient in the absence of lysis and grazing. FEMS Microbiol Ecol 85:443–451. https://doi.org/10.1111/1574-6941.12133.
45. Thompson LR, Zeng Q, Kelly L, Huang KH, Singer AU, Stubbe J, Chisholm SW. 2011. Phage auxiliary metabolic genes and the redirection of cyanobacterial host carbon metabolism. Proc Natl Acad Sci U S A 108:E757–E764. https://doi.org/10.1073/pnas.1102164108.
46. Frois-Moniz K. 2014. Host/virus interactions in the marine cyanobacterium Prochlorococcus. Ph.D. thesis. Massachusetts Institute of Technology, Cambridge, MA.
47. Nelson CE, Carlson CA. 2012. Tracking differential incorporation of dissolved organic carbon types among diverse lineages of Sargasso Sea bacterioplankton. Environ Microbiol 14:1500–1516. https://doi.org/10.1111/j.1462-2920.2012.02738.x.
48. Taylor JD, Cunliffe M. 2017. Coastal bacterioplankton community response to diatom-derived polysaccharide microgels. Environ Microbiol Rep 9:151–157. https://doi.org/10.1111/1758-2229.12513.
49. Gómez-Consarnau L, Lindh MV, Gasol JM, Pinhassi J. 2012. Structuring of bacterioplankton communities by specific dissolved organic carbon compounds. Environ Microbiol 14:2361–2378. https://doi.org/10.1111/j.1462-2920.2012.02804.x.
50. Ogawa H, Amagai Y, Koike I, Kaiser K, Benner R. 2001. Production of refractory dissolved organic matter by bacteria. Science 292:917–920. https://doi.org/10.1126/science.1057627.
51. Fasching C, Behounek B, Singer GA, Battin TJ. 2014. Microbial degradation of terrigenous dissolved organic matter and potential consequences for carbon cycling in brown-water streams. Sci Rep 4:4981. https://doi.org/10.1038/srep04981.
52. Faust K, Raes J. 2012. Microbial interactions: from networks to models. Nat Rev Microbiol 10:538–550. https://doi.org/10.1038/nrmicro2832.
53. Martínez-Pérez AM, Catalá TS, Nieto-Cid M, Otero J, Álvarez M, Emelianov M, Reche I, Álvarez-Salgado XA, Arístegui J. 2019. Dissolved organic matter (DOM) in the open Mediterranean Sea. II: Basin-wide distribution and drivers of fluorescent DOM. Prog Oceanogr 170:93–106. https://doi.org/10.1016/j.pocean.2018.10.019.
54. Biller SJ, Berube PM, Lindell D, Chisholm SW. 2015. Prochlorococcus: the structure and function of collective diversity. Nat Rev Microbiol 13:13–27. https://doi.org/10.1038/nrmicro3378.
55. Catalá TS, Reche I, Fuentes-Lema A, Romera-Castillo C, Nieto-Cid M, Ortega-Retuerta E, Calvo E, Alvarez M, Marrase C, Stedmon CA, Alvarez-Salgado XA. 2015. Turnover time of fluorescent dissolved organic matter in the dark global ocean. Nat Commun 6:5986. https://doi.org/10.1038/ncomms6986.
56. Kaplan A. 2016. Cyanophages: starving the host to recruit resources. Curr Biol 26:R511–R513. https://doi.org/10.1016/j.cub.2016.04.030.
57. Hurwitz BL, U'Ren JM. 2016. Viral metabolic reprogramming in marine ecosystems. Curr Opin Microbiol 31:161–168. https://doi.org/10.1016/j.mib.2016.04.002.
58. Sharma AK, Becker JW, Ottesen EA, Bryant JA, Duhamel S, Karl DM, Cordero OX, Repeta DJ, DeLong EF. 2014. Distinct dissolved organic matter sources induce rapid transcriptional responses in coexisting populations of *Prochlorococcus*, *Pelagibacter* and the OM60 clade. Environ Microbiol 16:2815–2830. https://doi.org/10.1111/1462-2920.12254.
59. Dadaglio L, Dinasquet J, Obernosterer I, Joux F. 2018. Differential responses of bacteria to diatom-derived dissolved organic matter in the Arctic Ocean. Aquat Microb Ecol 82:59–72. https://doi.org/10.3354/ame01883.
60. Jürgens K, Gasol JM, Vaqué D. 2000. Bacteria-flagellate coupling in microcosm experiments in the Central Atlantic Ocean. J Exp Mar Biol Ecol 245:127–147. https://doi.org/10.1016/S0022-0981(99)00156-2.
61. Zhang R, Weinbauer MG, Qian P-Y. 2007. Viruses and flagellates sustain apparent richness and reduce biomass accumulation of bacterioplankton in coastal marine waters. Environ Microbiol 9:3008–3018. https://doi.org/10.1111/j.1462-2920.2007.01410.x.
62. Gasol JM, Morán XAG. 1999. Effects of filtration on bacterial activity and picoplankton community structure as assessed by flow cytometry. Aquat Microb Ecol 16:251–264. https://doi.org/10.3354/ame016251.
63. Moore LR, Coe A, Zinser ER, Saito MA, Sullivan MB, Lindell D, Frois-Moniz K, Waterbury J, Chisholm SW. 2007. Culturing the marine cyanobacterium Prochlorococcus. Limnol Oceanogr Methods 5:353–362. https://doi.org/10.4319/lom.2007.5.353.
64. Bertilsson S, Berglund O, Karl DM, Chisholm SW. 2003. Elemental composition of marine Prochlorococcus and Synechococcus: implications for the ecological stoichiometry of the sea. Limnol Oceanogr 48:1721–1731. https://doi.org/10.4319/lo.2003.48.5.1721.
65. Wong GTF, Ku T-L, Mulholland M, Tseng C-M, Wang D-P. 2007. The SouthEast Asian Time-series Study (SEATS) and the biogeochemistry of the South China Sea—an overview. Deep Sea Res 2 Top Stud Oceanogr 54:1434–1447. https://doi.org/10.1016/j.dsr2.2007.05.012.
66. Lindroth P, Mopper K. 1979. High performance liquid chromatographic determination of subpicomole amounts of amino acids by precolumn fluorescence derivatization with o-phthaldialdehyde. Anal Chem 51:1667–1674. https://doi.org/10.1021/ac50047a019.
67. Li X, Liu Z, Chen W, Wang L, He B, Wu K, Gu S, Jiang P, Huang B, Dai M. 2018. Production and transformation of dissolved and particulate organic matter as indicated by amino acids in the Pearl River Estuary, China. J Geophys Res Biogeosci 123:3523–3537. https://doi.org/10.1029/2018JG004690.
68. Yamashita Y, Cory RM, Nishioka J, Kuma K, Tanoue E, Jaffe R. 2010. Fluorescence characteristics of dissolved organic matter in the deep waters of the Okhotsk Sea and the northwestern North Pacific Ocean. Deep Sea Res 2 Top Stud Oceanogr 57:1478–1485. https://doi.org/10.1016/j.dsr2.2010.02.016.
69. Spencer RGM, Hernes PJ, Ruf R, Baker A, Dyda RY, Stubbins A, Six J. 2010. Temporal controls on dissolved organic matter and lignin biogeochemistry in a pristine tropical river, Democratic Republic of Congo. J Geophys Res Atmos 30 https://doi.org/10.1029/2009JG001180.
70. Guo W, Yang L, Zhai W, Chen W, Osburn CL, Huang X, Li Y. 2014. Runoff-mediated seasonal oscillation in the dynamics of dissolved organic matter in different branches of a large bifurcated estuary—the Changjiang Estuary. J Geophys Res Biogeosci 119:776–793. https://doi.org/10.1002/2013JG002540.
71. Stedmon CA, Bro R. 2008. Characterizing dissolved organic matter fluorescence with parallel factor analysis: a tutorial. Limnol Oceanogr Methods 6:572–579. https://doi.org/10.4319/lom.2008.6.572.
72. Marie D, Partensky F, Vaulot D, Brussaard C. 1999. Enumeration of phytoplankton, bacteria, and viruses in marine samples. Curr Protoc Cytom 10:11.11.1–11.11.15. https://doi.org/10.1002/0471142956.cy1111s10.
73. Zhang R, Xia X, Lau SCK, Motegi C, Weinbauer MG, Jiao N. 2013. Response of bacterioplankton community structure to an artificial gradient of pCO_2 in the Arctic Ocean. Biogeosciences 10:3679–3689. https://doi.org/10.5194/bg-10-3679-2013.
74. Klindworth A, Pruesse E, Schweer T, Peplies J, Quast C, Horn M, Glöckner FO. 2013. Evaluation of general 16S ribosomal RNA gene PCR primers for classical and next-generation sequencing-based diversity studies. Nucleic Acids Res 41:e1. https://doi.org/10.1093/nar/gks808.
75. Magoč T, Salzberg SL. 2011. FLASH: fast length adjustment of short reads to improve genome assemblies. Bioinformatics 27:2957–2963. https://doi.org/10.1093/bioinformatics/btr507.
76. Caporaso JG, Kuczynski J, Stombaugh J, Bittinger K, Bushman FD,

Costello EK, Fierer N, Peña AG, Goodrich JK, Gordon JI, Huttley GA, Kelley ST, Knights D, Koenig JE, Ley RE, Lozupone CA, McDonald D, Muegge BD, Pirrung M, Reeder J, Sevinsky JR, Turnbaugh PJ, Walters WA, Widmann J, Yatsunenko T, Zaneveld J, Knight R. 2010. QIIME allows analysis of high-throughput community sequencing data. Nat Methods 7:335–336. https://doi.org/10.1038/nmeth.f.303.

77. Edgar RC, Haas BJ, Clemente JC, Quince C, Knight R. 2011. UCHIME improves sensitivity and speed of chimera detection. Bioinformatics 27:2194–2200. https://doi.org/10.1093/bioinformatics/btr381.
78. Edgar RC. 2013. UPARSE: highly accurate OTU sequences from microbial amplicon reads. Nat Methods 10:996–998. https://doi.org/10.1038/nmeth.2604.
79. Wang Q, Garrity GM, Tiedje JM, Cole JR. 2007. Naïve Bayesian classifier for rapid assignment of rRNA sequences into the new bacterial taxonomy. Appl Environ Microbiol 73:5261–5267. https://doi.org/10.1128/AEM.00062-07.
80. DeSantis TZ, Hugenholtz P, Larsen N, Rojas M, Brodie EL, Keller K, Huber T, Dalevi D, Hu P, Andersen GL. 2006. Greengenes, a chimera-checked 16S rRNA gene database and workbench compatible with ARB. Appl Environ Microbiol 72:5069–5072. https://doi.org/10.1128/AEM.03006-05.
81. Barberán A, Bates ST, Casamayor EO, Fierer N. 2012. Using network analysis to explore co-occurrence patterns in soil microbial communities. ISME J 6:343–351. https://doi.org/10.1038/ismej.2011.119.